

Uncovering Interpretable Internal States of Merging Tasks at Highway On-Ramps for Autonomous Driving Decision-Making

Huanjie Wang, Wenshuo Wang, *Member, IEEE*, Shihua Yuan, and Xueyuan Li

Abstract—Humans make daily routine decisions based on their internal states in intricate interaction scenarios. This paper presents a probabilistically reconstructive learning approach to identify the internal states of multi-vehicle sequential interactions when merging at highway on-ramps. We treated the merging task’s sequential decision as a dynamic, stochastic process and then integrated the internal states into an HMM-GMR model, a probabilistic combination of an extended Gaussian mixture regression (GMR) and hidden Markov models (HMM). We also developed a variant expectation-maximum (EM) algorithm to estimate the model parameters and verified it based on a real-world data set. Experiment results reveal that three interpretable internal states can semantically describe the interactive merge procedure at highway on-ramps. This finding provides a basis to develop an efficient model-based decision-making algorithm for autonomous vehicles (AVs) in a partially observable environment.

Note to Practitioners—Model-based learning approaches have obtained increasing attention in decision-making design due to their stability and interpretability. This paper was built upon the two facts: (1) Intelligent agents can only receive partially observable environment information directly through their equipped sensors in the real world; (2) Humans mainly utilize the internal states and associated dynamics inferred from observations to make proper decisions in complex environments. Similarly, AVs need to understand, infer, anticipate, and exploit the internal states of dynamic environments. Applying probabilistic decision-making models to AVs requires updating the internal states’ beliefs and associated dynamics after getting new observations. The designed and verified emission model in HMM-GMR provides a modifiable functional module for online updates of the associated internal states. Experiment results based on the real-world driving dataset demonstrates that the internal states extracted using HMM-GMR can represent the dynamic decision-making process semantically and make an accurate prediction.

Index Terms—Driver interaction behavior, internal state, hidden Markov model, Gaussian mixture regression, merge behavior.

I. INTRODUCTION

TAKING an efficient and safe merge at highway on-ramps is a daily-routine but challenging task for humans and autonomous agents in the real world [1]. Near 30,000 highway

This work is supported by the National Natural Science Foundation of China (Grant No. U1864210). (*Corresponding Authors: Wenshuo Wang and Shihua Yuan*)

H. Wang is with the School of Mechanical Engineering, Beijing Institute of Technology, Beijing 10081, China (e-mail: wanghj_815@163.com).

W. Wang is with the University of California at Berkeley, Berkeley, CA 94720 USA (e-mail: wwsbit@gmail.com).

S. Yuan and X. Li are with the School of Mechanical Engineering, Beijing Institute of Technology, Beijing 10081, China (e-mail: yuanshishua@bit.edu.cn).

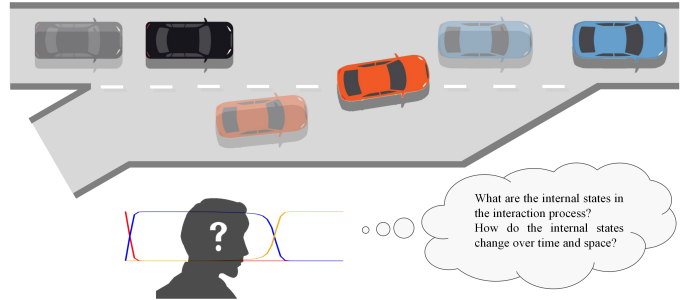


Fig. 1. The interaction of the ego vehicle (red) with its nearby surroundings (black and blue) when merging into the highway from on-ramps. The ego vehicle makes a proper decision based on its *internal* model of the dynamic environment.

merging collisions occurred per year in the USA [2]. Typical highway traffic issues such as oscillations, congestion, and speed breakdown are arising incrementally due to inefficient collaborations between the ego vehicle and its surroundings [3]. Thus, taking insights into humans’ cooperative merging processes in a changing context becomes indispensable to make a safer, more efficient decision for autonomous vehicles (AVs).

Humans can interact with non-stationary, separately controlled, and partially observable agents seamlessly but do not need to explicitly model each other’s strategy during the implementation of complex interaction processes [4]. Inspired by this, artificial agents (such as AVs) should make high-level strategy representations based on their observation of other agents’ low-level actions. The high-level strategy representation is implicit, known as *internal states*, which are usually changing over time [5]. The agents then take actions based on their previous choices of different plans or strategies. The low-level action is measurable; however, the other agents’ planning and internal state changes are unobservable but significant for the sequential decision process. When merging at highway on-ramps (as shown in Fig. 1), the human agent can directly detect the contextual traffic changes through their sensory dynamics, but not for the underlying states (such as intents) of the surrounding vehicles, which requires inference from the directly perceived signals. With this situation, the decision to merge in congested traffic involves a tremendous amount of cooperation, courtesy, and risk-taking and must explicitly consider the internal states’ change and influences [6].

The introduction of internal states allows to mathematically formulate many existing decision-making problems via

solvable, tractable mathematical models. A typical, popular decision-making model is built upon the Markov decision process (MDP), which basically describes the sequential decision-making mechanisms in complex interactive environments such as the merging procedure at highway on-ramps. One of its derivations, called partially observable MDP (POMDP), has been widely used to formulate the decision-making problem whose partial states are unobservable. Research in [7] defined the high-level discrete (internal) states of interactive merge behavior to formulate the decision-making into a solvable POMDP problem. Another typical model built upon MDP is deep reinforcement learning (Deep RL), which increases attention in the decision-making of autonomous driving when combined with deep neural networks [8]–[11]. However, the Deep RL strategy usually lacks interpretability and generalizability and can only adapt to well-defined and straightforward tasks. Besides, Deep RL requires learning the internal states through returns implicitly [12], being slow, sensitive to hyperparameters, and inefficient in practice [13]. A tractable alternative is to learn based on a well-predefined model (also called model-based methods) with explicit internal states. The use of explicit internal states makes the model definition interpretable and data utilization efficient [14]. Typical model-based approaches integrated with internal states include MDP [15], POMDP [16]–[18], and hidden Markov models (HMM) [19]. POMDP requires encoding the complete historical information¹ into possible *internal states* and makes an appropriate decision by evaluating the current observed state value while decoding the internal states. Therefore, the implementation of well-defined internal states can improve the learning efficiency and decision performance of algorithms.

Most existing research on internal states focuses on intention prediction of surrounding agents [12], [22]–[25] to provide the ego vehicle in-depth knowledge of the environment. However, they mainly focused on the internal state of each vehicle independently and assumed that the ego vehicle’s internal states are directly/closely related to their driving decision. All of them are subjectively defined but beyond rationality. It is also time-consuming and costly to manually specify the relevant internal states for complex dynamic environments since the flood of data and diversity in driving tasks can overwhelm human insight and analysis.

This paper provides a probabilistically learning approach to automatically extract the internal states of the multi-vehicle *interactive process* (rather than of a single vehicle’s behavior), which can guide the ego vehicle to make an appropriate decision. Based on the conclusion of our previous research in [26], we here developed a probabilistic approach (i.e., HMM-GMR) to learn and reproduce the internal dynamics of merge tasks at highway on-ramps. The proposed framework combines HMM with Gaussian mixture regression (GMR) [27] to leverage temporal information into dynamic processes. The GMR estimates the internal state and then predicts to verify the internal states’ effectiveness further. We also compared it to GMM-GMR that does *not* consider temporal information

¹Historical information can be encoded by recalling past features [20] or inferring the distribution over possible internal states [21].

into the dynamic process.

The remainder of this paper is organized as follows. Section II reviews related works on internal states. Section III discusses the real-world data collection and processing. Section IV introduces the HMM-GMR model. Section V analyzes the results and provides further discussions. Finally, Section VI gives the conclusions.

II. RELATED WORKS

This section first reviews the related works of internal states, ranging from driving style and driver intention to driving maneuver. Then, their limitations and the problem to be solved are summarized.

A. Internal States for Driving Style & Driver Intention

AVs must infer underlying states (e.g., driving styles and intents) of surrounding vehicles and their interactions to understand the environments fully [28]–[36]. To analyze aggressive driving and predict the driver intention, researchers in [30] treated the driving anger as a dynamic internal state and then built a hybrid model based on HMM. The inferred internal states can encode trajectories and distinguish different driver behaviors such as passive, aggressive, tailgater, and speeder [32]. Besides, the assigned internal state plays a critical role in the action selection. For example, to deeply understand the driving environment, research in [33] applied the Latent Dirichlet Allocation (LDA) model to discover the internal states of driving habits. Some researchers [35] also presented a learning-based framework to explicitly infer the internal states of surrounding vehicles (such as aggressive or conservative) using graph neural networks and demonstrated its superiority in complex scenarios such as intersections.

The intention estimation of surrounding vehicles can help to tackle dense interactions among agents in complex traffic scenarios [16], [24], [37]–[40]. For example, a multi-class support vector machine classifier combined with a Bayesian filter can predict the internal lane-change intention of surrounding drivers [38]. In order to guarantee the safety, efficiency, and smoothness of autonomous driving, Bai *et al.* proposed an intention-aware online planning approach to estimate pedestrian intentions and addressed the uncertainties in a complex environment [16]. The authors in [24] applied a probabilistic graphical model (PGM) to predict the internal intentions of surrounding vehicles in on-ramp merge scenarios. The structure of PGM allows embedding historical information and internal states into the system. Experimental results verified that the PGM-based approach can conservative personification and ensure the safety of the merging process. Considering the same observations could lead to different actions in complex scenarios (intersection or highway merge), Codevilla *et al.* [39] explicitly modelled the internal state by introducing information about the intentions and goals. In this way, the defined driver’s underlying internal state influenced the driver’s subsequent actions rather than the observations.

B. Internal States for Driving Maneuver/Behavior

In a real-world setting, AVs need to understand the surroundings and know the (internal) states of their maneuvers and behaviors. Considering the underlying (or internal) states and plans, Ben-Akiva, *et al.* [41] proposed an internal choice methodology for the highway on-ramp merge tasks in congested traffic and obtained an expected performance. Besides, Choudhury [22] introduced the internal plans into the decision process to address the decision-making problem in lane-change behaviors. Choudhury applied HMM to consider previous plans when making current decisions and demonstrated that ignorance of the internal states might cause an unrealistic understanding of the surrounding traffic environment. According to the internal states such as car-following, free-flow, emergency stop, the realization of a car-following maneuver consists of several actions such as acceleration, deceleration, and do-nothing [42]. Paschalidis *et al.* [43] modeled the stress level of the driver as the internal state and quantified its influence on decisions. Hsiao, *et al.* [44] trained a multi-modal policy using variational autoencoder to infer discrete internal states of different behaviors in mixed demonstrations. They verified the associated policy using the high-dimensional visual information as inputs. A multi-head network for learning internal states is also presented to predict relevant decision factors and address the limitations of high-dimensional images in data-scarce cases [45]. Also, Chen *et al.* explained whether and how the end-to-end network policy understands and responds to the environment by proposing an interpretable Deep RL with sequential internal states [46]. However, this approach is a model-free model that can not explain the decision-making process as explicitly as the model-based approach.

C. Summary

The above discussion indicates that the introduction of internal states in driving (such as driving style, driver intents, driver maneuver) enables safer and more efficient algorithms for AVs. However, the internal states combined with the probabilistic learning and inference approaches would require carefully defining the internal states in advance, challenging in complex driving settings. Moreover, although the learning-based models sometimes do not need to define the number and state in advance, it requires defining the reward function accurately, which is usually a function of the (internal) states [47]. Therefore, it is necessary to develop an approach that can systematically learn, define, and infer associated internal states while preserving interpretability.

III. DATASET AND DATA PROCESSING

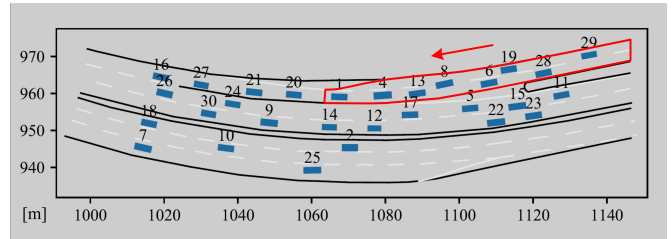
A. Real-World Dataset

We utilized the data collected from the real world – the INTERACTION dataset [48], with the following considerations:

- **Scenario diversity:** The data set covers great interactive driving scenarios, such as merging scenarios, intersections, and roundabouts.



(a) Real scene



(b) Data visualization

Fig. 2. The Chinese highway on-ramp merge scenario in the INTERACTION dataset [48] and the selected local region bounded by the red line.

- **Behavior diversity:** The data set collects regular and safe driving behaviors and highly interactive and complex driving behaviors, such as adversarial/irrational/near-collision maneuvers.
- **Clear definition:** The data set contains well-defined physical information, such as vehicles' position and speed in longitudinal and lateral directions, the corresponding timestamp with the resolution of 100 ms, agents' type (car or truck), yaw angle, as well as the length and width of vehicles.

B. Data Processing

The highway on-ramp merge scenarios contained in the INTERACTION dataset are from Chinese and German traffic, respectively. The video length of the Chinese (German) merge scenario is 94.62 (37.92) minutes, which contains 10359 (574) vehicles. As shown in Fig. 2, the upper two lanes of the Chinese merge scenario is selected because they contain a longer duration and a broader variety in driving behaviors.

The data processing is based on our previous research [26]. The definition of vehicles (i.e., ego vehicle, lead/lag vehicles), merge critical moments (i.e., start moment t_s , middle moment t_m , and end moment t_e), and social preference (rude or courteous) can refer to [26]. The sequential data during the whole process with courteous merging behavior between t_s and t_e are extracted and the merging event amounts to 789. The extracted data are then randomly divided into a training set (80% of the dataset) and a testing set (20% of the dataset). The merge event's duration is different from each other. To make the data suitable for HMM-GMR, we screened and re-aligned the extracted data by taking a trade-off between algorithm performance and calculation capability.

The variable selection in existing works usually relies on researchers' experience and onboard sensors [49], [50]. Our previous research [26] reveals that the critical variables change over the merging stages, and redundant variables should be removed as noises. Only proper variable selection can be

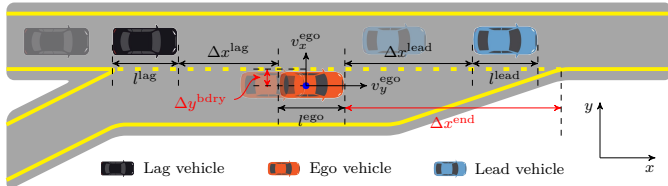


Fig. 3. Definition of variables for the highway on-ramp merge scenario.

conductive to the inference and learning of internal states and improve decision-making performance. According to the variables defined in Fig. 3, different tasks require selecting different variables. For model training and internal state inference, we defined the observation at time t as $\mathbf{x}_t = [\Delta v_x^{\text{lead}}, \Delta x^{\text{lag}}, v_x^{\text{ego}}, v_y^{\text{ego}}]^\top$. To verify the effectiveness of these learned internal states, we reconstructed some variables based on the internal state from an internal-state model and defined the inputs and outputs as

$$\mathbf{x}_t^I = \begin{bmatrix} \Delta v_x^{\text{lead}} \\ \Delta x^{\text{lag}} \\ v_x^{\text{ego}} \end{bmatrix}, \quad \mathbf{x}_t^O = v_y^{\text{ego}}$$

The evaluation of variable selection will be given in Section V-C.

IV. HMM-GMR MODEL

In this section, we developed an HMM-GMR framework to learn the internal states of the dynamic merge process from various demonstrations. We also build a probabilistic model to reproduce the sequential observations from these extracted internal states, thus verifying the model effectiveness. First, we will introduce the basis of HMM, including its framework and parameter estimation via the Baum–Welch algorithm. Then, we extended the traditional GMR to consider the spatial and sequential information contained in the HMM.

A. HMM for the Merge Task

For the merge process, we assume it is subject to a Markov chain – a mathematical model of a sequence of random variables that evolve over time in a probabilistic manner with the assumption: The value at next point in time only depends on the current state and not on what happened before. When executing complex tasks, human drivers make decisions not based on their directly-perceived signals, instead of on their unobservable internal understanding of the world. Therefore, we treated the internal modes as the discrete latent states subject to a Markov chain and the observations as the emissions of associated latent states. This operation allows formulating the merge task under a HMM framework. As a robust probabilistic method, HMM is good at dealing with spatial and temporal variabilities [51]. It can exhibit some degree of invariance to local warping (compression and stretching) of the time axis. A typical HMM is built on a discrete Markov model with a set of finite discrete latent states $z_t \in \mathcal{Z} = \{1, \dots, K\}$ and an associated observation model $p(\mathbf{x}_t|z_t)$. At time t , the observed

state \mathbf{x}_t , which only depends on the current latent state z_t at time t , is expressed as a Gaussian distribution

$$p(\mathbf{x}_t|z_t = k, \boldsymbol{\mu}_k, \boldsymbol{\Sigma}_k) \sim \mathcal{N}(\mathbf{x}_t|\boldsymbol{\mu}_k, \boldsymbol{\Sigma}_k) \quad (1)$$

where $\boldsymbol{\mu}_k$ and $\boldsymbol{\Sigma}_k$ represent the center vector and the covariance matrix of the k -th Gaussian distribution, respectively. Formulating the observation model as a Gaussian distribution is intuitive with the facts: Agents do not behave directly upon their sensory data because that data is merely an indirect observation of a hidden real-world [52], and the Gaussian distribution can be treated as a probabilistic model with latent states [53]. The Gaussian model parameter estimation is through the Maximum Likelihood Estimate (MLE).

Given the sequential observations $\mathbf{X} = \mathbf{x}_{1:T}$ ¹ and associated latent states $\mathbf{Z} = z_{1:T}$ with the Markov chain assumption, their joint probability distribution is derived by

$$p(\mathbf{X}, \mathbf{Z}|\boldsymbol{\theta}) = p(z_1|\boldsymbol{\pi}) \left[\prod_{t=2}^T p(z_t|z_{t-1}, \mathbf{A}) \right] \prod_{l=1}^T p(\mathbf{x}_l|z_l, \boldsymbol{\mu}, \boldsymbol{\Sigma}) \quad (2)$$

where unknown model parameters $\boldsymbol{\theta} = \{\boldsymbol{\pi}, \mathbf{A}, \boldsymbol{\mu}, \boldsymbol{\Sigma}\}$ need to be learned. $\boldsymbol{\pi} = \{\pi_k\}$ is the initial probability, the entries π_k represent the initial probability of being in state k . The first observation \mathbf{x}_1 could be assigned to one of the set of the latent states \mathcal{Z} with a categorical distribution $p(z_1|\boldsymbol{\pi})$. \mathbf{A} is the transition matrix, and the entries $A_{jk} = p(z_t = k|z_{t-1} = j)$ represent the probability of categorizing the current observation at time t as state k given the last observation at time $t-1$ being in state j with $0 \leq A_{jk} \leq 1$ with $\sum_j A_{jk} = 1$. Thus, \mathbf{A} can be denoted as

$$\mathbf{A} = \begin{pmatrix} A_{11} & \cdots & A_{1K} \\ \vdots & \ddots & \vdots \\ A_{K1} & \cdots & A_{KK} \end{pmatrix} \quad (3)$$

The procedure in (2) for the case of HMM is modified as follows. The corresponding observation \mathbf{x}_1 can be sampled based on the initial driving latent state z_1 with probabilities governed by π_k . The latent state of the next moment z_2 can be obtained according to the transition probabilities $p(z_2|z_1, \mathbf{A})$. Then, a sample for \mathbf{x}_2 and also z_3 can be drawn and so on. According to the generative procedure, our task becomes to estimate the probability of latent state sequences $z_{1:T}$ and the value of $\boldsymbol{\theta}$ that can best describe associated observation sequence $\mathbf{x}_{1:T}$. The following section will detail the related algorithms.

B. Parameter Learning

For a probabilistic model estimation with latent states involved, an effective way is to conduct estimation iteratively. One typical approach is the expectation-maximization (EM) algorithm which performs the maximum likelihood estimation of HMM. It alternates between estimating the values of latent states (E-step) and optimizing the model (M-step), then repeating these two steps until convergence. As a variant of the EM algorithm, the Baum–Welch algorithm [54], [55] can evaluate the parameters $\boldsymbol{\theta}$ of HMM efficiently.

¹We denote $\mathbf{x}_{1:T}$ as the shorthand of the sequence $\{\mathbf{x}_1, \dots, \mathbf{x}_T\}$.

1) *E-Step*: In the E-step, we fixed the estimated model parameter at the last iteration (denoted as θ^{old}) and then calculated the marginal probability distribution for latent state of occupying state k at time t , denoted as $\gamma_t(k) = p(z_t = k | \mathbf{X}, \theta^{\text{old}})$ and the posterior probability of transforming from latent state j at time $t-1$ to latent state k at time t , denoted as $\xi_t(j, k) = p(z_{t-1} = j, z_t = k | \mathbf{X}, \theta^{\text{old}})$. First, we determined the posterior distribution of the latent states $p(\mathbf{Z} | \mathbf{X}, \theta^{\text{old}})$ based on \mathbf{X} , the observation values and θ^{old} , the model parameters of the EM algorithm at last iteration. Then, we evaluated the expectation of the log-likelihood for the complete data as a function of θ

$$\begin{aligned} \mathcal{Q}(\theta, \theta^{\text{old}}) &= \sum_{\mathbf{Z}} p(\mathbf{Z} | \mathbf{X}, \theta^{\text{old}}) \ln p(\mathbf{X}, \mathbf{Z} | \theta) \\ &= \sum_{k=1}^K \gamma_1(k) \ln \pi_k + \sum_{t=2}^T \sum_{j=1}^K \sum_{k=1}^K \xi_t(j, k) \ln A_{jk} \\ &\quad + \sum_{t=1}^T \sum_{k=1}^K \gamma_t(k) \ln p(\mathbf{x}_t | \boldsymbol{\mu}_k, \boldsymbol{\Sigma}_k) \end{aligned} \quad (4)$$

Here, $\gamma_t(k)$ and $\xi_t(j, k)$ are evaluated via an efficient forward-backward algorithm [55]. The forward variable $\alpha_t(k)$ accounts for the joint probability of observing all the partial observation sequence $\mathbf{x}_{1:t}$ up to time t and occupying state k at time t is (see Appendix-A)

$$\alpha_t(k) = \mathcal{N}(\mathbf{x}_t | \boldsymbol{\mu}_k, \boldsymbol{\Sigma}_k) \sum_{m=1}^K \alpha_{t-1}(m) A_{mk} \quad (5)$$

with $\alpha_1(k) = \pi_k \mathcal{N}(\mathbf{x}_1 | \boldsymbol{\mu}_k, \boldsymbol{\Sigma}_k)$. Similarly, the backward variable $\beta_t(k)$ accounts for the conditional probability of all the future partial observation sequence $\mathbf{x}_{t+1:T}$ given the state k at time t is (see Appendix-B)

$$\beta_t(k) = \sum_{m=1}^K A_{km} \mathcal{N}(\mathbf{x}_{t+1} | \boldsymbol{\mu}_m, \boldsymbol{\Sigma}_m) \beta_{t+1}(m) \quad (6)$$

with $\beta_T(k) = 1$. Thus, we can separately update $\gamma_t(k)$ and $\xi_t(j, k)$ to be a probability measure, respectively, via

$$\begin{aligned} \gamma_t(k) &= \frac{\alpha_t(k) \beta_t(k)}{\sum_{m=1}^K \alpha_t(m) \beta_t(m)} \\ \xi_t(j, k) &= \frac{\alpha_{t-1}(j) A_{jk} \mathcal{N}(\mathbf{x}_t | \boldsymbol{\mu}_k, \boldsymbol{\Sigma}_k) \beta_t(k)}{\sum_{m=1}^K \sum_{n=1}^K \alpha_{t-1}(m) A_{mn} \mathcal{N}(\mathbf{x}_t | \boldsymbol{\mu}_n, \boldsymbol{\Sigma}_n) \beta_t(n)} \end{aligned} \quad (7)$$

2) *M-Step*: In the M-step, we updated the parameters θ by fixing the value of $\gamma_t(k)$ and $\xi_t(j, k)$ estimated in the E-step, thus optimizing the \mathcal{Q} -function alternately. More specifically, each element of $\boldsymbol{\pi}$ and \mathbf{A} are respectively maximized by

$$\begin{aligned} \pi_k &= \frac{\gamma_1(k)}{\sum_{j=1}^K \gamma_1(j)} \\ A_{jk} &= \frac{\sum_{t=2}^T \xi_t(j, k)}{\sum_{t=2}^T \sum_{n=1}^K \xi_t(j, n)} \end{aligned} \quad (8)$$

Besides, equation (4) shows that only its final term depends on $\boldsymbol{\mu}_k$ and $\boldsymbol{\Sigma}_k$ and has exactly the same form as the data-dependent term in the corresponding function for a standard

mixture distribution for independently identically distribution data. Therefore, by maximizing the function $\mathcal{Q}(\theta, \theta^{\text{old}})$ with a weighted version of the MLE of a multivariate Gaussian, we obtain the updates of $\boldsymbol{\mu}_k$ and $\boldsymbol{\Sigma}_k$ as

$$\boldsymbol{\mu}_k = \frac{\sum_{t=1}^T \gamma_t(k) \mathbf{x}_t}{\sum_{t=1}^T \gamma_t(k)} \quad (9)$$

$$\boldsymbol{\Sigma}_k = \frac{\sum_{t=1}^T \gamma_t(k) (\mathbf{x}_t - \boldsymbol{\mu}_k) (\mathbf{x}_t - \boldsymbol{\mu}_k)^\top}{\sum_{t=1}^T \gamma_t(k)} \quad (10)$$

The above E-step and M-step are performed alternatively until convergence, and the associated parameters θ are updated according to the latest estimation. The final obtained optimal parameters θ^* can be used to infer the *internal states* of the dynamic merge process.

C. Internal States in HMM-GMR

The above section introduces the HMM method to formulate the sequential observations with *latent states*. However, the learn latent states are not exactly equal to the *internal states* of the dynamic interaction process. The *internal states* should represent the dynamic interaction process and can rebuild and reproduce the associated behavior efficiently. Therefore, we define a probabilistic model based on the internal states to produce a distribution of associated behaviors.

Inspired by the fact that the reproduction of specific movement represented with GMMs can be formalized as a regression problem [56], we treated the above trained HMM with Gaussian-based emissions as a Gaussian mixture with certain sequential constraints. This alteration allows utilizing the Gaussian mixture regression (GMR) to retrieve associated behavior probabilistically. The retrieval performance corresponds to the representativeness of the learned *internal states*. Here, based on the learned HMM parameters $\theta = \{\boldsymbol{\pi}, \mathbf{A}, \boldsymbol{\mu}, \boldsymbol{\Sigma}\}$, we need to define the dynamic process of the internal states during the merging process. For a specific observation, we assume that several finite discrete potential internal states exist to be assigned, and each of them has different possibilities. Thus, the internal state, denoted by $h_k(\mathbf{x}_t^I)$, can be treated as a probability measure with $\sum_k h_k(\mathbf{x}_t^I) = 1$.

As claimed above, the appropriate internal state should be able to reproduce associated behavior precisely. Therefore, we can build a GMR model with these internal states integrated to evaluate the effectiveness. Unlike other regression methods such as artificial neural networks, locally weighted regression, and locally weighted projection regression, the GMR derives the regression function from the joint probability density function of the data rather than modeling the regression directly [27], [57]. The model training is then carried out offline, linearly related to the number of data points. The calculation of GMR is faster than other regression algorithms. Besides, GMR can handle multi-dimensional input and output variables under the same model architecture.

For the merge task at highway on-ramps, a critical variable that can reflect the driver intent is the ego vehicle's lateral speed, v_y^{ego} : A high (low) lateral speed indicates a strong (weak) intent to merge. Therefore, we treated the variable v_y^{ego}

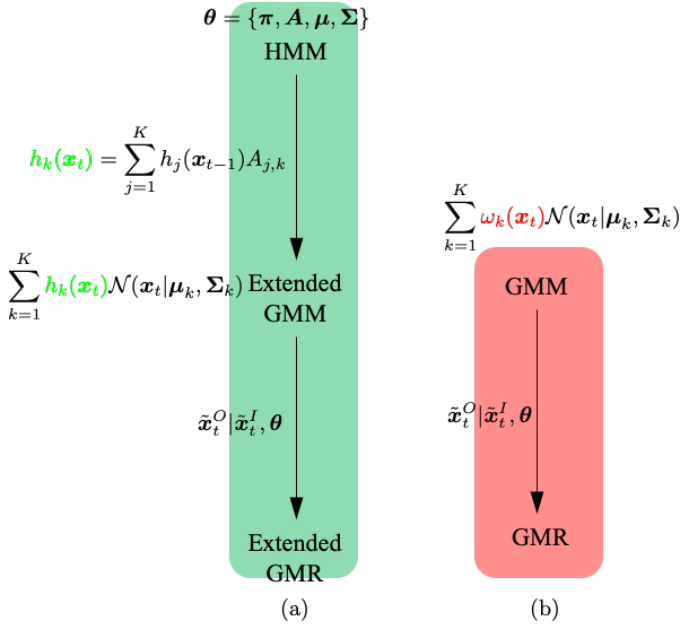


Fig. 4. Illustration of the frameworks of (a) HMM-GMR and (b) GMM-GMR.

as the output of GMR and the other variables as the inputs of GMR. In what follows, the superscripts I and O , which represent the exponents for matrices or vectors, are used to distinguish between input and output. In what follows, we use the block decomposition of data x as

$$x = \begin{bmatrix} x^I \\ x^O \end{bmatrix} \quad (11)$$

where x^I and x^O represent the inputs and output defined in Section III-B, respectively.

The representation of each observation in HMM depends on the previous choices and is jointly determined by the different components and their probabilities. Thus, HMM can be interpreted as an extended mixture model and its parameters can also be applied in GMR. More specifically, the distribution of any observation x falling in the k -th state of HMM can thus be expressed as a multivariate Gaussian with mean and covariance

$$\mu_k = \begin{bmatrix} \mu_k^I \\ \mu_k^O \end{bmatrix}, \Sigma_k = \begin{bmatrix} \Sigma_k^{II} & \Sigma_k^{IO} \\ \Sigma_k^{OI} & \Sigma_k^{OO} \end{bmatrix} \quad (12)$$

We decompose the mean vector and covariance matrix corresponding to the block decomposition in (11). Equation (12) implies that the joint distribution of the inputs and output is a Gaussian distribution. According to [58], for any new input \tilde{x}_t^I , the associated output \tilde{x}_t^O is also a multimodal distribution conditional on the estimated model parameters by

$$\tilde{x}_t^O | \tilde{x}_t^I, \theta \sim \sum_{k=1}^K h_k(\tilde{x}_t^I) \mathcal{N}(\hat{\mu}_k^O, \hat{\Sigma}_k^{OI}) \quad (13)$$

with the weights $h_k(\tilde{x}_t^I)$ and

$$\begin{aligned} \hat{\mu}_k^O(\tilde{x}_t^I) &= \mu_k^O + \Sigma_k^{OI} (\Sigma_k^{II})^{-1} (\tilde{x}_t^I - \mu_k^I) \\ \hat{\Sigma}_k^{OI} &= \Sigma_k^{OO} - \Sigma_k^{OI} (\Sigma_k^{II})^{-1} \Sigma_k^{IO} \end{aligned} \quad (14)$$

The conditional probability distribution function of the observations is the weighted summation of different components in the mixture Gaussian at each time step t .

Fig. 4(b) illustrates that the traditional development of GMR relies on a parameterized GMM, and the weights ω_k corresponding to each Gaussian component represent the associated influence on the input data but independent of time and sequence [56]. In our case, we need to first transfer the well-trained HMM with Gaussian-based emissions as an extended Gaussian mixture model. Unlike in the traditional GMM, we need to consider the influence of previous observation one step ahead on the current observation when estimating $h_k(x_t)$, as shown in Fig. 4(a). The likelihood of current observation x_t belongs to component k (i.e., $h_k(x_t)$) is estimated as the expectation of the likelihood of the previous observation x_{t-1} belong to all components $j = 1, \dots, K$ with a transition probability $A_{j,k}$. Therefore, to make the extended GMR like HMM leveraging the spatial and sequential information, the likelihood function $h_k(\tilde{x}_t)$ is estimated recursively with the HMM representation. Thus, the weights $h_k(\tilde{x}_t^I)$ in (13) are derived as

$$h_k(\tilde{x}_t^I) = \frac{\left(\sum_{m=1}^K h_m(\tilde{x}_{t-1}^I) A_{mk} \right) \mathcal{N}(\tilde{x}_t^I | \mu_k^I, \Sigma_k^{II})}{\sum_{n=1}^K \left(\sum_{m=1}^K h_m(\tilde{x}_{t-1}^I) A_{mn} \right) \mathcal{N}(\tilde{x}_t^I | \mu_n^I, \Sigma_n^{II})} \quad (15)$$

corresponds to the probability of observing the partial sequence $\tilde{x}_{1:t}$ and of being in state k at time t , where $h_k(\tilde{x}_t^I)$ is the forward variable of HMM. When $t = 1$, the initial value is set by

$$h_k(\tilde{x}_1^I) = \frac{\pi_k \mathcal{N}(\tilde{x}_1^I | \mu_k^I, \Sigma_k^{II})}{\sum_{n=1}^K \pi_n \mathcal{N}(\tilde{x}_1^I | \mu_n^I, \Sigma_n^{II})}$$

Equation (13) provides the full predictive probability density of the HMM-GMR approach and can predict the distribution of outputs given any input. Equation (15) is a probability measure and represents the likelihood of the current observation belong to the k -th Gaussian component, which can be interpreted as the human's *internal* beliefs to how likely the current observation falling into the given states.

The defined internal states' reproductive capability can evaluate their correctness. According to the definition of internal states, the expectation with the probability of the well-learned internal states should be as close as possible to the actual measurement. Therefore, we provide a point prediction result by evaluating the expectations of the estimated conditional centers $\hat{\mu}^O(\tilde{x}_t^I)$

$$\hat{\mu}^O(\tilde{x}_t^I) = \sum_{k=1}^K h_k(\tilde{x}_t^I) \hat{\mu}_k^O(\tilde{x}_t^I) \quad (16)$$

A small deviation to (16) indicates a good performance.

V. RESULT ANALYSIS AND DISCUSSION

This section first introduces the structure learning for HMM and then defines two evaluation metrics to assess the variable selection and the HMM-GMR performance. Afterward, the analysis of learned internal states and related potential applications are provided.

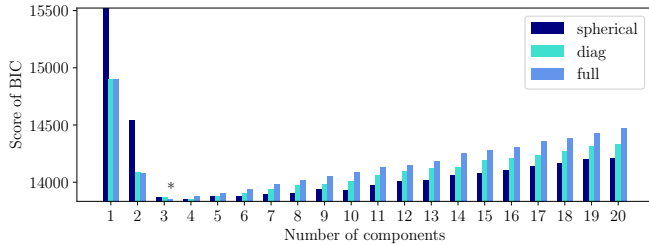


Fig. 5. The BIC scores of GMM with different components K .

A. Model Selection

The Baum–Welch algorithm (introduced in Section IV) is a variant of the EM algorithms, which requires determining the number of components K for GMM in advance. The optimal model parameter K is determined by gradually increasing the number of components and selecting the optimum based on off-the-shelf criteria called Bayesian information criteria (BIC) [59], [60], balancing the model’s likelihood and the minimum parameter number. The computation of the BIC score is given by

$$S_{\text{BIC}} = - \sum_{t=1}^T \log(p(\mathbf{x}_t)) + \frac{n_p}{2} \log(T) \quad (17)$$

where the first term represents the log-likelihood and determines the fitting level of the model to the data. The second penalty factor realizes the number minimization of parameters with n_p the number of parameters that can be calculated by polynomials about K . $\{\mathbf{x}_t\}$ is the set of training data point, and T represents the number of data.

For the model selection, we calculate the BIC scores with different components from 1 to 20, as shown in Fig. 5. It indicates that the BIC score first decreases and goes up with increasing K . This suggests that the mixture model with $K = 3$ (marked with *) is the optimal selection to achieve the best performance while minimizing the parameter number. Therefore, considering the states/clusters in the framework are multivariate normal distributions with a full covariance matrix, the mixture model with 3 Gaussian components is optimal for describing real-world driving data.

B. Performance Evaluation

The model performance is evaluated using the mean-square error (MSE) and root-mean-square error (RMSE). The MSE describes the unbiased estimation of the error variance, computed by

$$\epsilon_{\text{MSE}} = \frac{1}{T} \sum_{t=1}^T (\hat{x}_t^O - x_t^O)^2 \quad (18)$$

where $\hat{x}_t^O = \hat{\boldsymbol{\mu}}^O(\tilde{\mathbf{x}}_t^I)$ is the estimation of output variable at time t and computed via (16). x_t^O is the real reference value collected from sensor. Therefore, the associated evaluation score of MSE is computed as [61]

$$S_{\text{MSE}} = \frac{\epsilon_{\text{MSE}} - \epsilon_{\text{MSE}}^{\text{ref}}}{0 - \epsilon_{\text{MSE}}^{\text{ref}}} \quad (19)$$

with $\epsilon_{\text{MSE}}^{\text{ref}} = \frac{1}{T} \sum_{t=1}^T (\bar{x} - x_t^O)^2$. Taking the MSE of \bar{x} as the reference, the overall performance can be evaluated by the score of S_{MSE} which is positive (negative) if the predictive outputs is better (worse) than $\epsilon_{\text{MSE}}^{\text{ref}}$ while the absolute value of the score is proportional to the amplitude.

In addition, we use RMSE as another evaluation metric, computed by

$$\epsilon_{\text{RMSE}} = \sqrt{\epsilon_{\text{MSE}}} \quad (20)$$

Thus, the mean values of two evaluation metrics (\bar{S}_{MSE} and $\bar{\epsilon}_{\text{RMSE}}$) are used to evaluate the prediction stability and accuracy of the HMM-GMR performance. A high value of \bar{S}_{MSE} (or a low value of $\bar{\epsilon}_{\text{RMSE}}$) indicates a good model performance.

C. Evaluation of Variable Selection

The selection of appropriate input variables can eliminate the interference of redundant variables and maximize the performance of the HMM-GMR framework. Our previous research in [26] reveals that the most critical variables of making decisions when merging into the highway are ranked as v_y^{ego} , v_x^{ego} , Δv_x^{lead} , Δx^{lag} , Δv_x^{lag} , and Δx^{lead} (TTC is not considered because the correlation between it and task execution is weak and unstable). v_y^{ego} represents the lateral control of the ego vehicle (i.e., the predictive outputs of HMM-GMR); thus, we only selected the other five variables as the model input candidates.

With well-defined evaluation metrics, we compute the evaluation scores of models with different variable inputs. Here, we mainly consider the univariate input of the top-three significant variables (i.e., Δv_x^{lead} , Δx^{lag} and v_x^{ego}). For those variables with low significance, we only discuss the influence of different combinations of them with the optimal input on model performance. Table I summarizes the associated results by combining different variables. It shows that the input variables as the combination of $\{\Delta v_x^{\text{lead}}, \Delta x^{\text{lag}}, v_x^{\text{ego}}\}$ is the best choice with the highest value of \bar{S}_{MSE} and the lowest value of $\bar{\epsilon}_{\text{RMSE}}$.

Besides, we also investigated the other combinations, provided as follows:

- **Combining univariate inputs:** Table I indicates that Δv_x^{lead} reaches a much higher value of \bar{S}_{MSE} than the other two combinations. However, Δv_x^{lead} obtains a close value of $\bar{\epsilon}_{\text{RMSE}}$ to Δx^{lag} , which are both far worse than v_x^{ego} .
- **Combining bivariate inputs:** The combination of Δx^{lag} and v_x^{ego} obtains the best performance with the highest value of \bar{S}_{MSE} and the lowest value of $\bar{\epsilon}_{\text{RMSE}}$. Δv_x^{lead} is excluded in this case because the the bivariate inputs’ coupling effect is different from the univariate inputs.

The evaluation scores of the univariate and bivariate inputs reveal that insufficient inputs can undermine model performance.

To further confirm the reliability of the optimal combination of the three variables as inputs, we also analyzed the effects of the optimal combination (i.e., $\Delta v_x^{\text{lead}}, \Delta x^{\text{lag}}, v_x^{\text{ego}}$) with other low-significant variables (i.e., $\Delta v_x^{\text{lag}}, \Delta x^{\text{lead}}$). The associated results in Table I show that the introduction of low-significant

TABLE I
PERFORMANCE EVALUATION OF DIFFERENT VARIABLES WITH SAME APPROACH (HMM-GMR (K -BINS)) AND OUTPUT VARIABLE (v_y^{ego})

| Input variables | \bar{S}_{MSE} | \bar{e}_{RMSE} |
|----------------------------------------------------------------------------------------------------------------------|------------------------|-------------------------|
| Δv_x^{lead} | 0.346 | 0.608 |
| Δx^{lag} | -1.665 | 0.685 |
| v_x^{ego} | -0.261 | 0.124 |
| $\Delta v_x^{\text{lead}}, \Delta x^{\text{lag}}$ | -0.067 | 0.148 |
| $\Delta v_x^{\text{lead}}, v_x^{\text{ego}}$ | 0.525 | 0.075 |
| $\Delta x^{\text{lag}}, v_x^{\text{ego}}$ | 0.631 | 0.062 |
| $\Delta v_x^{\text{lead}}, \Delta x^{\text{lag}}, v_x^{\text{ego}}$ | 0.686 | 0.059 |
| $\Delta v_x^{\text{lead}}, \Delta x^{\text{lag}}, v_x^{\text{ego}}, \Delta v_x^{\text{lag}}$ | 0.591 | 0.065 |
| $\Delta v_x^{\text{lead}}, \Delta x^{\text{lag}}, v_x^{\text{ego}}, \Delta x^{\text{lead}}$ | 0.458 | 0.065 |
| $\Delta v_x^{\text{lead}}, \Delta x^{\text{lag}}, v_x^{\text{ego}}, \Delta v_x^{\text{lag}}, \Delta x^{\text{lead}}$ | 0.344 | 0.070 |

TABLE II
PERFORMANCE EVALUATION OF DIFFERENT APPROACHES WITH SAME INPUT VARIABLES ($\Delta v_x^{\text{lead}}, \Delta x^{\text{lag}}, v_x^{\text{ego}}$) AND OUTPUT VARIABLE v_y^{ego}

| Approach (Initialization method) | \bar{S}_{MSE} | \bar{e}_{RMSE} |
|----------------------------------|------------------------|-------------------------|
| HMM-GMR (K -bins) | 0.686 | 0.059 |
| HMM-GMR (K -means) | 0.604 | 0.061 |
| GMM-GMR (K -bins) | 0.485 | 0.065 |
| GMM-GMR (K -means) | 0.329 | 0.066 |

variables would undermine the model performance gradually since \bar{S}_{MSE} gets a reduced value, and \bar{e}_{RMSE} gets an increased value. Especially for the last case in Table I, the value of \bar{S}_{MSE} declines when considering the two low-significant variables mentioned above. This phenomenon supports the conclusion of variable significance analysis in [26], implying that considering low-significant variables will impair model performance. Therefore, it is necessary to filter redundant variables in the environment to improve the model performance.

D. Evaluation of Prediction Results

The analysis of variable selection in the previous section shows that the combination of $\{\Delta v_x^{\text{lead}}, \Delta x^{\text{lag}}, v_x^{\text{ego}}\}$ is optimal and then used to eliminate the interference of redundant variables on decision-making performance. To evaluate the proposed HMM-GMR performance, we compare it with its counterpart of GMM-GMR defined in Fig. 4(b). Unlike the HMM-GMR, the weight coefficients ω of different Gaussian models in GMM-GMR in the iteration procedure are independent of time and sequence. Corresponding to (15) in HMM-GMR, the activation in GMM-GMR for state k at time step t is defined as follows

$$h_k(\mathbf{x}_t^I) = \frac{\omega_k \mathcal{N}(\mathbf{x}_t^I | \boldsymbol{\mu}_k^I, \boldsymbol{\Sigma}_k^{II})}{\sum_{n=1}^K \omega_n \mathcal{N}(\mathbf{x}_t^I | \boldsymbol{\mu}_n^I, \boldsymbol{\Sigma}_n^{II})} \quad (21)$$

The model parameters should be initialized by proper initialization to avoid being trapped in poor local minima. In the training and testing processes, we introduced two different initialization methods:

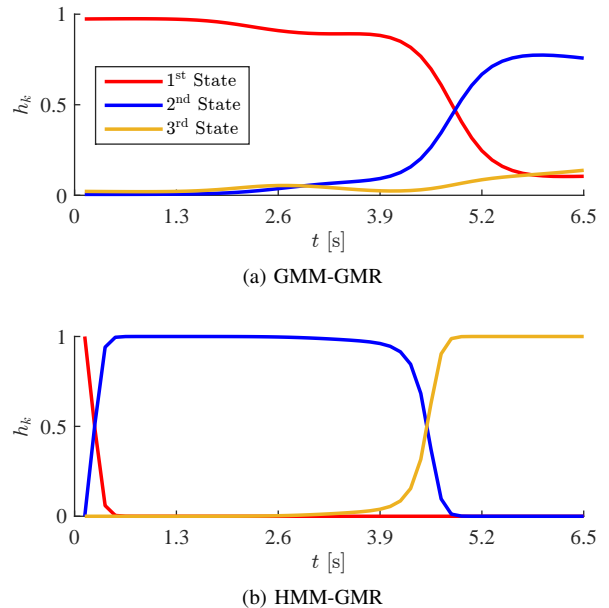


Fig. 6. The activation weights h_k (internal state) derived by GMM-GMR and HMM-GMR for one case.

- K -means: initialize the model parameters by using K -means clustering algorithm; and
- K -bins: initialize the model parameters by clustering an ordered dataset into equal bins.

Table II displays the evaluation results and indicates that HMM-GMR outperforms GMM-GMR, reaching a higher value of \bar{S}_{MSE} and a lower value of \bar{e}_{RMSE} than GMM-GMR. Moreover, both HMM-GMR and GMM-GMR with initialization of K -bins always obtain a better performance than using K -means. Besides, Fig. 6 displays that the update of internal states based on GMM-GMR is more oscillating than HMM-GMR because GMM-GMR does not leverage the influence of time and sequence in the learning and testing phases. As a result, it leads to a large prediction error, making the internal states obtained by the activation function of GMM-GMR is not as stable as HMM-GMR. By considering the factors mentioned above comprehensively, we can conclude that the HMM-GMR framework initializing with K -bins obtains the best performance. This evidence proves that the internal state obtained via HMM-GMR is close to the actual situation.

The above analysis allows treating $\{\Delta v_x^{\text{lead}}, \Delta x^{\text{lag}}, v_x^{\text{ego}}\}$ as the inputs of HMM-GMR with K -bins initialization. Figs. 7 and 8 display the training (based on all the training cases) and testing (one randomly selected test case) results, respectively. Each figure shows the results from two views: two-dimensional view (bottom) and three-dimensional view (top). The two-dimensional view is a plane diagram of the relationship between the input variable v_x^{ego} and the output variable v_y^{ego} . The training results (as shown in Fig. 7) display the relationships between the three Gaussian components and all the training data, while the testing results in Fig. 8 indicate that the HMM-GMR model can obtain a good prediction performance.

Figs. 7 and 8 display that the red Gaussian component (i.e., the first internal state) covers the most wider range over the

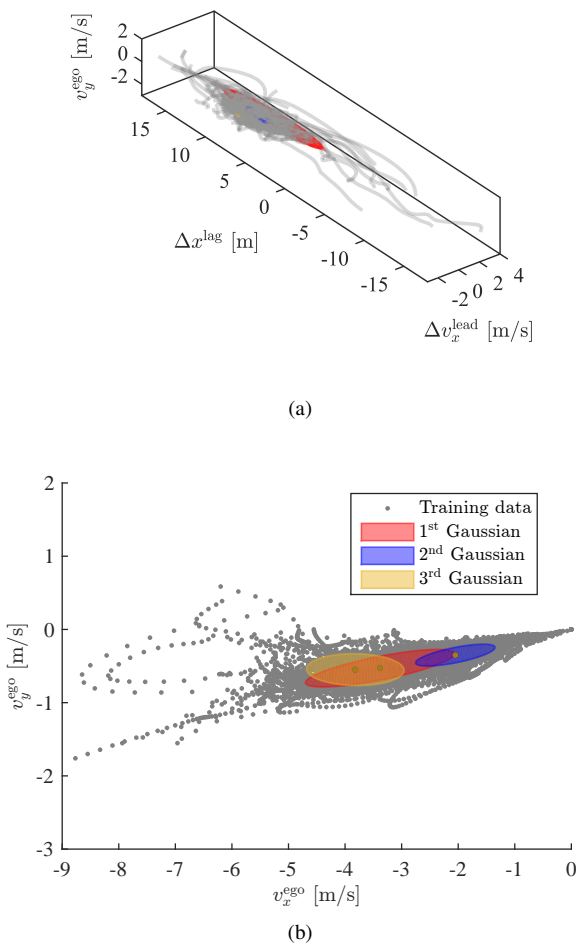


Fig. 7. Training results of HMM-GMR.

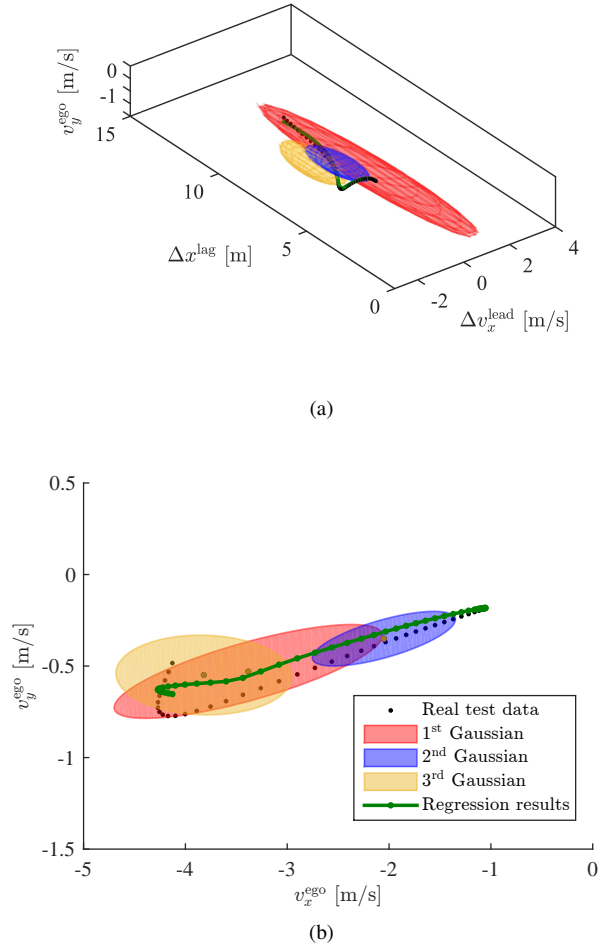


Fig. 8. Example of the testing result for a randomly selected test case.

three independent variables, while the blue Gaussian component (i.e., the second internal state) obtains the narrowest one. The randomness of the relative relationship between the ego vehicle and the surrounding agents is strong, while the relative relationship is more regular and concentrated in the second internal state. Besides, with the increase of v_x^{ego} , the regularity of training data gradually weakens; that is, the test error increases with the increase of v_x^{ego} . The reasons for this phenomenon are analyzed in Section V-F2.

E. Interpretability of Internal State

This section will interpret the learned internal states of the merging behavior at highway on-ramps semantically. According to the update of the activation coefficient in Fig. 6b, Fig. 9 displays how the internal states correspond to the merging procedure over time.

To interpret the interaction behavior during the merging task with the three learned internal states, we listed the range of each internal state for each input variable in Table III. All collected vehicle speed is non-positive because all vehicles in the dataset drive toward the left direction, as shown in Fig. 2. Table III indicates that the ego vehicle’s absolute speed

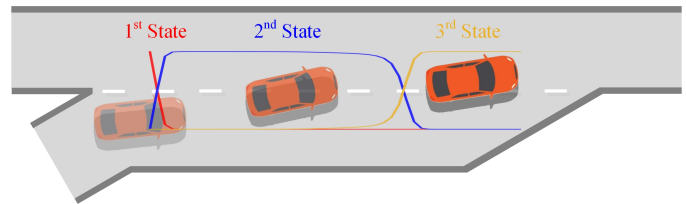


Fig. 9. An example of the internal state changes during the merging process.

first decreases and then gradually increases. However, the speed difference between the lead vehicle and the ego vehicle decreases and finally remains non-positive from the second state. From the second state, the ego vehicle moves slower than the lead vehicle. Although the ego vehicle gradually accelerates, it always moves slower than the lead vehicle to keep a safe distance from the lead vehicle. Besides, the distance between the lag vehicles and the ego vehicles first decreases and then increases, indicating that after the second state, the rear vehicle would actively increase the safety distance to the ego vehicle. The dynamic interactions reflected by the corresponding relationship between the internal states and the selected variables are consistent with the highway on-ramp merge behavior in reality. Therefore, the three learned

TABLE III
THE RANGES OF INPUT VARIABLES IN DIFFERENT INTERNAL STATES

| | | 1 st State | 2 nd State | 3 rd State |
|----------------------------|-------|-----------------------|-----------------------|-----------------------|
| Δv_x^{lead} | [m/s] | [-0.7, 1.2] | [-1.1, 0.0] | [-1.7, -0.2] |
| v_x^{ego} | [m/s] | [-4.7, -2.0] | [-2.8, -1.4] | [-4.7, -2.9] |
| Δx^{lag} | [m] | [-0.4, 11.6] | [4.8, 8.2] | [5.4, 9.1] |

internal states can fully and concretely explain the interactive merge behavior.

F. Further Discussions

1) *Potential Applications:* Model-based RL and POMDP receive increasing attention in recent years [16]–[18] in light of their interpretability and generalizability [14]. POMDP usually treats the unobservable environmental uncertainty as internal states or considers the complete historical information encoded by recalling past features and inferring to determine the distribution over possible internal states [21]. Although the belief state’s rationality in POMDP has found some evidence in recent experimental studies [62], the update of this belief state requires the state transition and observation function. The HMM-GMR framework developed in this paper can provide the basic parameter update procedures for model-based approaches to improve learning efficiency and decision performance.

2) *Limitations:* Most highway on-ramp merging scenarios in the INTERACTION dataset are in a congested, highly interactive condition. The developed HMM-GMR framework obtains an expected prediction performance and infers the internal states during the decision process. However, the model trained with this kind of data may not be suitable for the free-flow traffic conditions, which could be future work.

VI. CONCLUSION

This paper developed a probabilistic learning approach, HMM-GMR, to extract the interpretable internal states for the dynamic interaction procedure of merging at highway on-ramps. Related parameter estimation algorithms for the HMM-GMR model are provided. Experiments on the real-world data demonstrate its efficiency and reveal that the interaction procedure for merge behavior at highway on-ramps can be semantically described via three internal states. We also evaluated the HMM-GMR model with different variables as inputs. We demonstrated that the optimal model inputs are $\{\Delta v_x^{\text{lead}}, \Delta x^{\text{lag}}, v_x^{\text{ego}}\}$ to make an appropriate decision. Moreover, the developed HMM-GMR model, to some extent, provides reliable and experimental support to the conclusions in our previous work [26].

APPENDIX

A. Derivation of Forward Variable $\alpha_t(k)$

For the forward variable $\alpha_t(k)$, its estimation is based on the old parameter θ^{old} , i.e., $\alpha_t(k) = p(\mathbf{x}_{1:t}, z_t = k | \theta^{\text{old}})$. To

simplify the proof representation, we omitted the parameter θ^{old} and default $p(\mathbf{x}_{1:t}, z_t = k | \theta^{\text{old}}) = p(\mathbf{x}_{1:t}, z_t = k)$.

$$\begin{aligned}
\alpha_t(k) &= p(\mathbf{x}_{1:t}, z_t = k) \\
&= p(\mathbf{x}_t | z_t = k) p(\mathbf{x}_{1:t-1} | z_t = k) p(z_t = k) \\
&= p(\mathbf{x}_t | z_t = k) p(\mathbf{x}_{1:t-1}, z_t = k) \\
&= p(\mathbf{x}_t | z_t = k) \sum_{m=1}^K p(\mathbf{x}_{1:t-1}, z_{t-1} = m, z_t = k) \\
&= p(\mathbf{x}_t | z_t = k) \sum_{m=1}^K [p(\mathbf{x}_{1:t-1}, z_t = k | z_{t-1} = m) \cdot \\
&\quad p(z_{t-1} = m)] \\
&= p(\mathbf{x}_t | z_t = k) \sum_{m=1}^K [p(\mathbf{x}_{1:t-1}, z_{t-1} = m) \cdot \\
&\quad p(z_t = k | z_{t-1} = m)] \\
&= p(\mathbf{x}_t | z_t = k, \boldsymbol{\mu}_k, \boldsymbol{\Sigma}_k) \sum_{m=1}^K \alpha_{t-1}(m) A_{mk} \\
&= \mathcal{N}(\mathbf{x}_t | \boldsymbol{\mu}_k, \boldsymbol{\Sigma}_k) \sum_{m=1}^K \alpha_{t-1}(m) A_{mk}
\end{aligned}$$

B. Derivation of Backward Variable $\beta_t(k)$

The estimation of backward variable $\beta_t(k)$ is based on the old parameter θ^{old} , i.e., $\beta_t(k) = p(\mathbf{x}_{t+1:T} | z_t = k, \theta^{\text{old}})$. To simplify the proof representation, we omitted the parameter θ^{old} and default $p(\mathbf{x}_{t+1:T} | z_t = k, \theta^{\text{old}}) = p(\mathbf{x}_{t+1:T} | z_t = k)$.

$$\begin{aligned}
\beta_t(k) &= p(\mathbf{x}_{t+1:T} | z_t = k) \\
&= \sum_{m=1}^K p(\mathbf{x}_{t+1:T}, z_{t+1} = m | z_t = k) \\
&= \sum_{m=1}^K [p(z_{t+1} = m | z_t = k) \cdot \\
&\quad p(\mathbf{x}_{t+1:T} | z_t = k, z_{t+1} = m)] \\
&= \sum_{m=1}^K [p(z_{t+1} = m | z_t = k) p(\mathbf{x}_{t+1:T} | z_{t+1} = m)] \\
&= \sum_{m=1}^K [p(z_{t+1} = m | z_t = k) p(\mathbf{x}_{t+1} | z_{t+1} = m) \cdot \\
&\quad p(\mathbf{x}_{t+2:T} | z_{t+1} = m)] \\
&= \sum_{m=1}^K A_{km} p(\mathbf{x}_{t+1} | z_{t+1} = m, \boldsymbol{\mu}_m, \boldsymbol{\Sigma}_m) \beta_{t+1}(m) \\
&= \sum_{m=1}^K A_{km} \mathcal{N}(\mathbf{x}_{t+1} | \boldsymbol{\mu}_m, \boldsymbol{\Sigma}_m) \beta_{t+1}(m)
\end{aligned}$$

REFERENCES

- [1] Y. Lin, J. McPhee, and N. L. Azad, “Decision-making and control for freeway on-ramp merging using deep reinforcement learning,” *arXiv preprint arXiv:1909.12967*, 2019.

- [2] N. H. T. S. Administration, "Summary of motor vehicle crashes: 2016 data," United States. National Highway Traffic Safety Administration, Tech. Rep., 2018.
- [3] F. Marczak, W. Daamen, and C. Buisson, "Merging behaviour: Empirical comparison between two sites and new theory development," *Transportation Research Part C: Emerging Technologies*, vol. 36, pp. 530–546, 2013.
- [4] A. Rubinstein, *Modeling bounded rationality*. MIT press, 1998.
- [5] A. Xie, D. P. Losey, R. Tolsma, C. Finn, and D. Sadigh, "Learning latent representations to influence multi-agent interaction," *arXiv preprint arXiv:2011.06619*, 2020.
- [6] C. F. Choudhury, M. Ben-Akiva, and M. Abou-Zeid, "Dynamic latent plan models," *Journal of Choice Modelling*, vol. 3, no. 2, pp. 50–70, 2010.
- [7] C. Hubmann, J. Schulz, G. Xu, D. Althoff, and C. Stiller, "A belief state planner for interactive merge maneuvers in congested traffic," in *2018 21st International Conference on Intelligent Transportation Systems (ITSC)*. IEEE, 2018, pp. 1617–1624.
- [8] J. R. N. Forbes, *Reinforcement learning for autonomous vehicles*. University of California, Berkeley, 2002.
- [9] A. E. Sallab, M. Abdou, E. Perot, and S. Yogamani, "Deep reinforcement learning framework for autonomous driving," *Electronic Imaging*, vol. 2017, no. 19, pp. 70–76, 2017.
- [10] W. Zhang, K. Song, X. Rong, and Y. Li, "Coarse-to-fine uav target tracking with deep reinforcement learning," *IEEE Transactions on Automation Science and Engineering*, vol. 16, no. 4, pp. 1522–1530, 2018.
- [11] H. Wang, S. Yuan, M. Guo, C.-Y. Chan, X. Li, and W. Lan, "Tactical driving decisions of unmanned ground vehicles in complex highway environments: A deep reinforcement learning approach," *Proceedings of the Institution of Mechanical Engineers, Part D: Journal of Automobile Engineering*, vol. 235, no. 4, pp. 1113–1127, 2021.
- [12] T. Matisen, A. Labash, D. Majoral, J. Aru, and R. Vicente, "Do deep reinforcement learning agents model intentions?" *arXiv preprint arXiv:1805.06020*, 2018.
- [13] A. Lee, A. Nagabandi, P. Abbeel, and S. Levine, "Stochastic latent actor-critic: Deep reinforcement learning with a latent variable model," *Advances in Neural Information Processing Systems*, vol. 33, 2020.
- [14] J. Chen, Z. Xu, and M. Tomizuka, "End-to-end autonomous driving perception with sequential latent representation learning," *arXiv preprint arXiv:2003.12464*, 2020.
- [15] M. J. Kochenderfer, *Decision making under uncertainty: theory and application*. MIT press, 2015.
- [16] H. Bai, S. Cai, N. Ye, D. Hsu, and W. S. Lee, "Intention-aware online pomdp planning for autonomous driving in a crowd," in *2015 IEEE International Conference on Robotics and Automation (ICRA)*. IEEE, 2015, pp. 454–460.
- [17] M. Hausknecht and P. Stone, "Deep recurrent q-learning for partially observable mdps," *arXiv preprint arXiv:1507.06527*, 2015.
- [18] W. Song, G. Xiong, and H. Chen, "Intention-aware autonomous driving decision-making in an uncontrolled intersection," *Mathematical Problems in Engineering*, vol. 2016, 2016.
- [19] L. E. Baum *et al.*, "An inequality and associated maximization technique in statistical estimation for probabilistic functions of markov processes," *Inequalities*, vol. 3, no. 1, pp. 1–8, 1972.
- [20] R. A. McCallum, "Overcoming incomplete perception with utile distinction memory," in *Proceedings of the Tenth International Conference on Machine Learning*, 1993, pp. 190–196.
- [21] L. P. Kaelbling, M. L. Littman, and A. R. Cassandra, "Planning and acting in partially observable stochastic domains," *Artificial Intelligence*, vol. 101, no. 1-2, pp. 99–134, 1998.
- [22] C. F. Choudhury, "Modeling driving decisions with latent plans," Ph.D. dissertation, Massachusetts Institute of Technology, 2007.
- [23] S. Lefevre, A. Carvalho, and F. Borrelli, "A learning-based framework for velocity control in autonomous driving," *IEEE Transactions on Automation Science and Engineering*, vol. 13, no. 1, pp. 32–42, 2015.
- [24] C. Dong, J. M. Dolan, and B. Litkouhi, "Intention estimation for ramp merging control in autonomous driving," in *2017 IEEE Intelligent Vehicles Symposium (IV)*. IEEE, 2017, pp. 1584–1589.
- [25] D. Hafner, T. Lillicrap, I. Fischer, R. Villegas, D. Ha, H. Lee, and J. Davidson, "Learning latent dynamics for planning from pixels," in *International Conference on Machine Learning*. PMLR, 2019, pp. 2555–2565.
- [26] H. Wang, W. Wang, S. Yuan, X. Li, and L. Sun, "On social interactions of merging behaviors at highway on-ramps in congested traffic," *arXiv preprint arXiv:2008.06156*, 2020.
- [27] S. Calinon, F. D'Halluin, E. Sauser, D. Caldwell, and A. Billard, "Learning and reproduction of gestures by imitation: An approach based on hidden markov model and gaussian mixture regression," *robotics & automation magazine IEEE*, vol. 17, no. 2, pp. 44–54, 2010.
- [28] T. Bär, D. Nienhüser, R. Kohlhaas, and J. M. Zöllner, "Probabilistic driving style determination by means of a situation based analysis of the vehicle data," in *2011 14th International IEEE Conference on Intelligent Transportation Systems (ITSC)*. IEEE, 2011, pp. 1698–1703.
- [29] B. Higgs and M. Abbas, "A two-step segmentation algorithm for behavioral clustering of naturalistic driving styles," in *16th International IEEE Conference on Intelligent Transportation Systems (ITSC 2013)*. IEEE, 2013, pp. 857–862.
- [30] M. Danaf, M. Abou-Zeid, and I. Kaysi, "Modeling anger and aggressive driving behavior in a dynamic choice-latent variable model," *Accident Analysis & Prevention*, vol. 75, pp. 105–118, 2015.
- [31] W. Dong, J. Li, R. Yao, C. Li, T. Yuan, and L. Wang, "Characterizing driving styles with deep learning," *arXiv preprint arXiv:1607.03611*, 2016.
- [32] J. Morton and M. J. Kochenderfer, "Simultaneous policy learning and latent state inference for imitating driver behavior," in *2017 IEEE 20th International Conference on Intelligent Transportation Systems (ITSC)*. IEEE, 2017, pp. 1–6.
- [33] Z. Chen, Y. Zhang, C. Wu, and B. Ran, "Understanding individualization driving states via latent dirichlet allocation model," *IEEE Intelligent Transportation Systems Magazine*, vol. 11, no. 2, pp. 41–53, 2019.
- [34] H. Gao, J. Zhu, T. Zhang, G. Xie, Z. Kan, Z. Hao, and K. Liu, "Situational assessment for intelligent vehicles based on stochastic model and gaussian distributions in typical traffic scenarios," *IEEE Transactions on Systems, Man, and Cybernetics: Systems*, 2020.
- [35] X. Ma, J. Li, M. J. Kochenderfer, D. Isele, and K. Fujimura, "Reinforcement learning for autonomous driving with latent state inference and spatial-temporal relationships," *arXiv preprint arXiv:2011.04251*, 2020.
- [36] H. Gao, F. Guo, J. Zhu, Z. Kan, and X. Zhang, "Human motion segmentation based on structure constraint matrix factorization," *Inform. Sci.*, vol. 2022, no. 65, p. 119103, 2022.
- [37] H. Berndt, J. Emmert, and K. Dietmayer, "Continuous driver intention recognition with hidden markov models," in *2008 11th International IEEE Conference on Intelligent Transportation Systems*. IEEE, 2008, pp. 1189–1194.
- [38] P. Kumar, M. Perrollaz, S. Lefevre, and C. Laugier, "Learning-based approach for online lane change intention prediction," in *2013 IEEE Intelligent Vehicles Symposium (IV)*. IEEE, 2013, pp. 797–802.
- [39] F. Codevilla, M. Müller, A. López, V. Koltun, and A. Dosovitskiy, "End-to-end driving via conditional imitation learning," in *2018 IEEE International Conference on Robotics and Automation (ICRA)*. IEEE, 2018, pp. 4693–4700.
- [40] H. Gao, H. Su, Y. Cai, R. Wu, Z. Hao, Y. Xu, W. Wu, J. Wang, Z. Li, and Z. Kan, "Trajectory prediction of cyclist based on dynamic bayesian network and long short-term memory model at unsignalized intersections," *SCIENCE CHINA Information Sciences*, 2020.
- [41] M. Ben-Akiva, C. Choudhury, and T. Toledo, "Modeling latent choices: application to driving behavior," in *11th International Conference on Travel Behaviour Research, Kyoto, Japan*, vol. 1620, 2006, p. 431470.
- [42] H. N. Koutsopoulos and H. Farah, "Latent class model for car following behavior," *Transportation research part B: methodological*, vol. 46, no. 5, pp. 563–578, 2012.
- [43] E. Paschalidis, C. F. Choudhury, and S. Hess, "Combining driving simulator and physiological sensor data in a latent variable model to incorporate the effect of stress in car-following behaviour," *Analytic methods in accident research*, vol. 22, p. 100089, 2019.
- [44] F.-I. Hsiao, J.-H. Kuo, and M. Sun, "Learning a multi-modal policy via imitating demonstrations with mixed behaviors," *arXiv preprint arXiv:1903.10304*, 2019.
- [45] E. Kargar and V. Kyriki, "Efficient latent representations using multiple tasks for autonomous driving," *arXiv preprint arXiv:2003.00695*, 2020.
- [46] J. Chen, S. E. Li, and M. Tomizuka, "Interpretable end-to-end urban autonomous driving with latent deep reinforcement learning," *arXiv preprint arXiv:2001.08726*, 2020.
- [47] Y. Niv, "Learning task-state representations," *Nature neuroscience*, vol. 22, no. 10, pp. 1544–1553, 2019.
- [48] W. Zhan, L. Sun, D. Wang, H. Shi, A. Clause, M. Naumann, J. Kummerle, H. Königshof, C. Stiller, A. de La Fortelle *et al.*, "Interaction dataset: An international, adversarial and cooperative motion dataset in interactive driving scenarios with semantic maps," *arXiv preprint arXiv:1910.03088*, 2019.

- [49] D. Li and H. Gao, "A hardware platform framework for an intelligent vehicle based on a driving brain," *Engineering*, vol. 4, no. 4, pp. 464–470, 2018.
- [50] H. Gao, J. Zhu, X. Li, Y. Kang, J. Li, and H. Su, "Automatic parking control of unmanned vehicle based on switching control algorithm and backstepping," *IEEE/ASME Transactions on Mechatronics*, 2020.
- [51] D. Trabelsi, S. Mohammed, F. Chamroukhi, L. Oukhellou, and Y. Amirat, "An unsupervised approach for automatic activity recognition based on hidden markov model regression," *IEEE Transactions on automation science and engineering*, vol. 10, no. 3, pp. 829–835, 2013.
- [52] Z. Wu, M. Kwon, S. Daptardar, P. Schrater, and X. Pitkow, "Rational thoughts in neural codes," *Proceedings of the National Academy of Sciences*, vol. 117, no. 47, pp. 29 311–29 320, 2020.
- [53] C. M. Bishop, *Pattern recognition and machine learning*. Springer, 2006.
- [54] L. E. Baum, T. Petrie, G. Soules, and N. Weiss, "A maximization technique occurring in the statistical analysis of probabilistic functions of markov chains," *The annals of mathematical statistics*, vol. 41, no. 1, pp. 164–171, 1970.
- [55] L. R. Rabiner, "A tutorial on hidden markov models and selected applications in speech recognition," *Proceedings of the IEEE*, vol. 77, no. 2, pp. 257–286, 1989.
- [56] Z. Ghahramani and M. Jordan, "Supervised learning from incomplete data via an em approach," *Advances in neural information processing systems*, vol. 6, pp. 120–127, 1993.
- [57] W. Shao, Z. Ge, L. Yao, and Z. Song, "Bayesian nonlinear gaussian mixture regression and its application to virtual sensing for multimode industrial processes," *IEEE Transactions on Automation Science and Engineering*, vol. 17, no. 2, pp. 871–885, 2019.
- [58] K. P. Murphy, *Machine learning: a probabilistic perspective*. MIT press, 2012.
- [59] G. Schwarz *et al.*, "Estimating the dimension of a model," *The annals of statistics*, vol. 6, no. 2, pp. 461–464, 1978.
- [60] S. Watanabe, "A widely applicable bayesian information criterion," *Journal of Machine Learning Research*, vol. 14, no. Mar, pp. 867–897, 2013.
- [61] R. H. McCuen, Z. Knight, and A. G. Cutter, "Evaluation of the nash–sutcliffe efficiency index," *Journal of hydrologic engineering*, vol. 11, no. 6, pp. 597–602, 2006.
- [62] B. M. Babayan, N. Uchida, and S. J. Gershman, "Belief state representation in the dopamine system," *Nature communications*, vol. 9, no. 1, pp. 1–10, 2018.



ground vehicle.

Shihua Yuan received the B.S., M.S., and Ph.D. degrees in vehicle engineering from the Beijing Institute of Technology, Beijing, China, in 1982, 1985, and 2000, respectively. From 1992 to 1997, he was an Associate Professor with the Beijing Institute of Technology, where he has been a Professor with the School of Mechanical Engineering, since 1997. He is the author of more than 100 research articles. His research interests include vehicle dynamics, vehicle braking energy recovery, vehicle continuous transmission and its control technology, and unmanned



Huanjie Wang received the M.A. degree from the School of Mechanical Engineering, Beijing Institute of Technology (BIT), China, in 2016, where he is currently pursuing the Ph.D. degree in mechanical engineering. He was also a Research Scholar with the University of California at Berkeley (UCB) from 2018 to 2020. His research interests include automated vehicle, situational awareness, decision-making, and machine learning.



ory and technology, unmanned vehicle theory and technology, and machine learning.

Xueyuan Li received the B.S., M.S., and Ph.D. degrees in vehicle engineering from the Beijing Institute of Technology, Beijing, China, in 1999, 2002, and 2010, respectively. He was the Director of the National Key Laboratory of Vehicular Transmission, from 2008 to 2014. He is currently the Vice Director of the Department of Vehicle Engineering, Beijing Institute of Technology. Since 2002, he has been an Associate Professor with the School of Mechanical Engineering, Beijing Institute of Technology. His research interests include vehicle transmission theory and technology, unmanned vehicle theory and technology, and machine learning.



Ann Arbor, from 2017 to 2018. His research interests include Bayesian nonparametric learning, human driver model, human–vehicle interaction, ADAS, and autonomous vehicles.

Wenshuo Wang (SM'15–M'18) received the Ph.D. degree in mechanical engineering from the Beijing Institute of Technology, Beijing, China, in 2018. He is currently working as a Postdoctoral Researcher with California Partners for Advanced Transportation Technology (California PATH), UC Berkeley. He was a Postdoctoral Research Associate with the Carnegie Mellon University, Pittsburgh, PA, USA, from 2018 to 2019. He was also a Research Scholar with the University of California at Berkeley from 2015 to 2017 and with the University of Michigan,